



# Influence of Initial Stress and Deformation States on the Shear Creep Behavior of Rock Discontinuities with Different Joint Roughness Coefficients

Zhen Wang<sup>1</sup> · Linlin Gu<sup>2</sup> · Qingzhao Zhang<sup>3,4</sup> · Bo-An Jang<sup>5</sup>

Received: 23 March 2021 / Accepted: 24 August 2021 / Published online: 3 September 2021  
© The Author(s), under exclusive licence to Springer-Verlag GmbH Austria, part of Springer Nature 2021

## Abstract

The sliding of rock blocks along rock discontinuities is caused by accumulated deformation and can result in disasters such as rock bursts and earthquakes. Creep along rock discontinuities leads to the accumulation of sliding deformation and random instability over time. The initial stress and deformation are important factors that strongly influence creep behavior. To investigate the influence of the initial state on the creep behavior of rock discontinuities, shear creep tests with loading–unloading shear pre-stress paths and shear creep tests with different initial stress and deformation states were conducted on artificial rock discontinuity samples prepared according to Barton’s standard roughness profiles. The creep behavior characteristics were investigated in detail according to the initial stress and deformation conditions. The results show that the initial stress and deformation states, which are related to crack development and plastic deformation accumulation, strongly influence creep behavior. Larger initial stress and deformation produce lower creep deformation, creep rates, and accelerated velocities. Samples with higher joint roughness coefficients produce more noticeable creep because more asperities provide additional space for creep to occur. A limit curve is also proven to exist, which allows the stress–deformation coordinate system to be divided into stable and unstable regions. When the current stress state of a sample is insufficient to drive the formation of further cracks or deformation in the rock discontinuity, the deformation and stress remain stable and no further creep is observed.

**Keywords** Creep · Rock discontinuity · Initial stress · Deformation · Joint roughness coefficient

✉ Bo-An Jang  
bajang@kangwan.ac.kr

Zhen Wang  
wangzhen2012@njust.edu.cn

Linlin Gu  
linlin\_gu@njust.edu.cn

Qingzhao Zhang  
zqz0726@163.com

<sup>1</sup> School of Mechanical Engineering, Nanjing University of Science and Technology, Nanjing 210094, China

<sup>2</sup> Department of Civil Engineering, Nanjing University of Science and Technology, Nanjing 210094, China

<sup>3</sup> Key Laboratory of Geotechnical and Underground Engineering of Ministry of Education, Tongji University, Shanghai 200092, China

<sup>4</sup> Department of Geotechnical Engineering, Tongji University, Shanghai 200092, China

<sup>5</sup> Department of Geophysics, Kangwon National University, 1 Kangwondaehak-gil, Chuncheon-si, Gangwon-do 24341, Republic of Korea

## List of Symbols

$\tau$	Shear stress
$\tau_{cs}$	Creep stress
$\tau_s$	Shear strength
$\tau_1$	Maximum stress in the loading section
$\tau_i$	Internal resistance
$D$	Shear deformation
$D_c$	Creep deformation
$D_i$	Instantaneous deformation prior to the shear creep stage
$\Delta D$	Equivalent plastic deformation before creep
$a$	Accelerated velocity
$a_i$	Initial accelerated velocity
$t$	Time
$v_c$	Creep rate at the end of the steady creep stage
$m$	Block quality
$S$	Shear area
$m_c, n_c$	Fitting parameters

## 1 Introduction

Rock discontinuities (e.g., joints, stratifications, faults) divide a rock mass into blocks. The sliding of rock blocks along rock discontinuities can cause sliding rock bursts, collapses, and earthquakes (Gomberg et al. 2011; Araki et al. 2017). For example, fault sliding caused by mining activities at the Witwatersrand gold mine in South Africa resulted in multiple seismic events with a maximum magnitude of 5.1 (Fernandez and Van der Heever 1984; Durrheim et al. 1998). The sliding of rock blocks mainly depends on the accumulation of deformation along rock discontinuities (Zhou et al. 2015a, b; Wang et al. 2015). The shear creep deformation of rock discontinuities is the main form of deformation accumulation under high and long-term stress, which leads to time-lag characteristics of the sliding rock blocks. Time-lag rock bursts were monitored at the Jinping hydropower station in China and the maximum lag time for excavation was found to be 163 days. This type of rock burst is closely related to the sliding of rock blocks along rock discontinuities (Chen et al. 2012). However, the occurrence uncertainty conceals precursory disaster characteristics, which makes it very difficult to provide early warnings and predict disasters.

Shear creep is an important time-dependent behavior of rock discontinuities. Asanov and Pan'kov (2004) performed shear creep tests on salt rock joints and observed three stages in the shear creep of rock discontinuities: transient creep stage; steady creep stage; and accelerating creep stage. Shear creep characteristics are influenced by many factors including the creep stress, normal stress, contact area, surface roughness, and moisture content (Drescher and Handley 2003; Wang et al. 2015). The characteristics of creep deformation and creep rates depend on the ratio of creep stress to shear strength (Zhang et al. 2011). Shear creep tests have shown that the total creep deformation increases with increasing roughness of the rock discontinuity and normal stress (Wang et al. 2018). Li et al. (2008) conducted shear creep tests and showed that the moisture content also influences creep characteristics and creep deformation. Creep rates increase with increasing moisture content owing to the lubrication, softening, and argillization effects of water.

The initial stress and deformation states are also important factors that influence creep behavior. Stress paths prior to creep or disturbances during creep cause variation in the initial stress and deformation states of the subsequent creep. Extensive research has been conducted to investigate the influence of disturbances on rock creep. Malan et al. (1997) and Malan (1999) monitored creep deformation in mining practices after blasting and reported that blasting produced additional instantaneous deformation

and changed the stress and deformation states of the rock mass. A continuous pattern was observed where a primary decelerating closure phase was monitored over a period of a few hours, followed by a steady creep deformation phase until the next blast occurred. Gao et al. (2017) performed laboratory tests to investigate the perturbation effect of rock rheology tests. The strain threshold of the ultimate failure strain was approximately 90%, which was used as the dividing point between the perturbation-sensitive and non-sensitive areas. The test results of Zhu et al. (2019) and Wang et al. (2020a) indicate that dynamic disturbances may introduce further damage and deformation in rock and shorten the time to failure owing to creep. The stress path prior to creep (hereafter referred to as the pre-stress path) also influences the initial stress and deformation state and strongly affects the creep characteristics. However, the influence of the initial state on the shear creep behavior of rock discontinuities has received little research attention, even though it is closely related to the occurrence of time-lag earthquakes and rockbursts.

Rock discontinuities may experience complex pre-stress paths, such as high and long-term geostress (loading) and unloading or disturbances caused by excavation. Different initial states lead to different creep behavior in rock discontinuities. To address this question, shear creep tests were conducted on samples with artificial joint surfaces based on Barton's ten standard roughness profiles using a loading–unloading shear stress path to produce differences in the initial stress and creep deformation states. The characteristics of creep under the influence of different initial stress and deformation states caused by the loading–unloading stress paths were investigated and the effect of the initial state was analyzed. Multi-stage creep tests coupled with loading–unloading stress paths were also conducted. The influence mechanism of the initial state on the subsequent creep was also studied and preliminary results regarding the limit curve and stable and unstable regions were obtained.

## 2 Methodology

### 2.1 Test Equipment

A servo-controlled rheological testing device was used to conduct shear creep tests with different stress paths (Fig. 1a). The maximum compressive loads in the vertical and horizontal directions were 500 and 300 kN, respectively, measured by normal and horizontal force transducers with an accuracy of 0.1 N. The stress steps were programmed in advance and the entire test process was controlled using a computer and servo controller. A load can be applied using the horizontal and vertical loading system (sections D and E in Fig. 1a) through the platens as shown in Fig. 1b. The load

**Fig. 1** Test apparatus (A: normal force transducer; B: horizontal force transducer; C: servo controller; D: horizontal loading system; E: vertical loading system; F: linear variable displacement transducers/ LVDT)

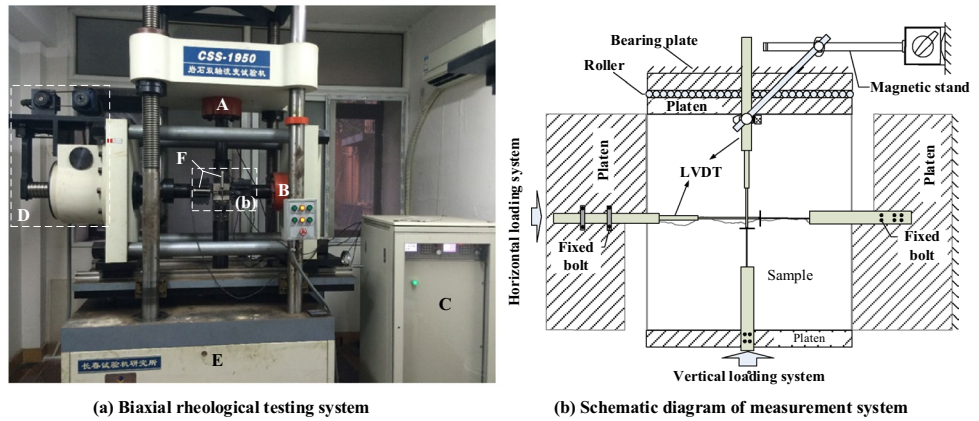


**Table 1** Physical–mechanical parameters of the cement-mortar

Uniaxial compression strength (MPa)	Elastic modulus (GPa)	Density (g/cm <sup>3</sup> )	Poisson's ratio	Cohesion (MPa)	Friction angle (°)
21.73	7.9	2.05	0.23	4.05	49.23°

can be maintained constantly for more than 1000 h without interruption. When the load is applied, the block slides along the rock discontinuity, and the friction between the platen and the bearing plate of the loading system is greatly reduced by the rollers. Deformation and stress data can be simultaneously monitored and calculated. The vertical and horizontal deformation were measured by two linear variable displacement transducers, as shown in Fig. 1b. The measurement error was controlled to within 0.5%. The accuracy of the deformation measurement was 1 μm in the range of 0–10 mm. In each direction, the deformation was calculated by averaging the two measurements. The temperature was controlled at 20 ± 1 °C and the relative humidity was maintained at 50 ± 2%, using a constant-temperature humidistat to eliminate any effects of temperature and moisture fluctuations on the sample or equipment.

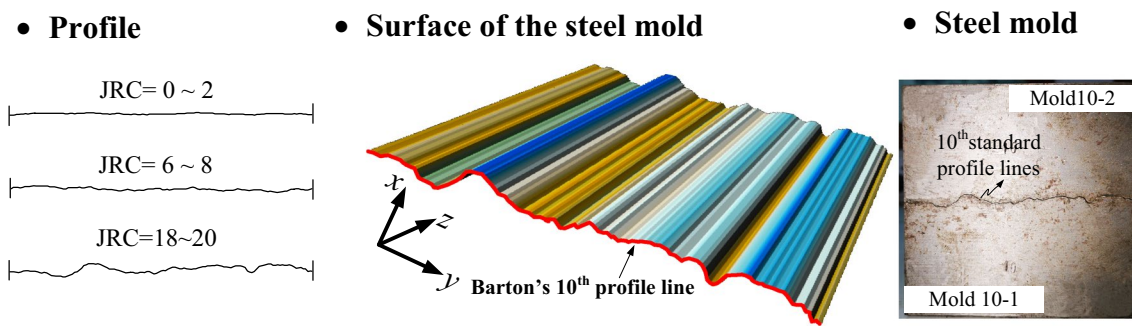
**2.2 Sample Preparation**

Cement mortar is a rock-like material that is widely used to simulate rock discontinuities and test their mechanical properties (Einstein et al. 1983; Li et al. 2006; Wang et al. 2020b). The samples in this study were cast using a mixture of water, Portland cement (#325), and sand with a fineness modulus of 1.8 and bulk density of 1450 kg/m<sup>3</sup>. The mixture proportion was 1:2:4. The physical–mechanical parameters of the cement mortar were obtained from physical property tests, uniaxial compression tests, and triaxial compression tests in accordance with the International Society for

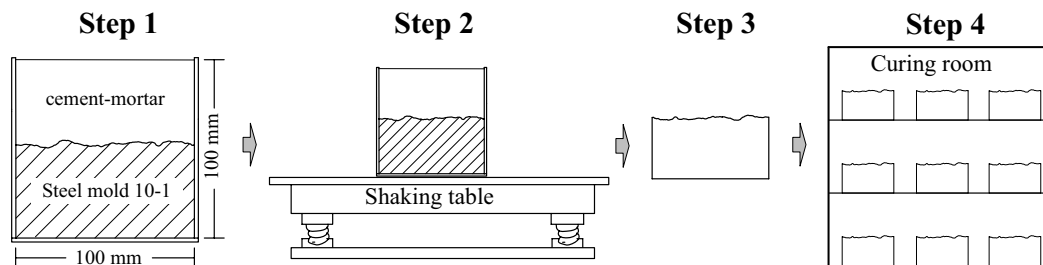
Rock Mechanics (Ulusay 2015). The results are presented in Table 1.

Barton's standard roughness profiles were chosen to prepare cement-mortar samples with discontinuities (Barton 1973; Barton and Choubey 1977). The samples were cube-shaped with dimensions of 10 × 10 × 10 cm and prepared using a steel mold with a morphology of the first [joint roughness coefficients (JRC)=0–2], fourth (JRC = 6–8), and tenth (JRC = 18–20) Barton's standard roughness profiles. As shown in Fig. 2a, the two-dimensional (2D) Barton's standard profile line (xy plane) is shifted along the normal direction of the 2D section (z-axis) to form a three-dimensional (3D) surface. The steel molds were manufactured using a computer-controlled machine with an accuracy of 0.1 μm in a mold vendor based on the above 3D surface. The steel mold for each sample contains two pieces, which form both sides of the rock discontinuity (Fig. 2). The steel mold for Barton's 10th standard profile line contains molds 10-1 and 10-2. Mold 10-1 was manufactured using the 10th standard profile and mold 10-2 was made by conversion of the profile. The two pieces therefore match perfectly. The sample preparation process is shown in Fig. 2. The cement mortar was stirred thoroughly and poured into the steel mold in three batches. The cement mortar was fully shaken each time to discharge large bubbles. The vibration time was controlled strictly and the vibration rehabilitation was timely. When free mortar appeared on the concrete surface and did not sink any more, the vibration was stopped, the remaining mortar was poured into the steel mold, and the mold was vibrated again. The free mortar with bubbles was scraped flat after each episode of vibration. The samples were removed from the mold 24 h later and stored in a standard curing room for 28 days. The temperature and humidity of the curing room were approximately 20 ± 1 °C and 95%, respectively.

Direct shear tests were conducted on samples with different JRC values. In the tests, a normal stress of 6.52 MPa (30% of uniaxial compression strength) was applied, and



(a) Steel mold and surface of the steel mold



(b) Sample preparation process

Fig. 2 Preparation method for rock sample with artificial joint surface (Wang et al. 2020a, b)

Table 2 Shear stress of the shear creep tests with loading–unloading stress path before creep

Sample	$\tau_1$ (MPa)	$\tau_{cs}$ (MPa)	$\tau_s$ (MPa)
JRC = 1	2.82, 3.29, 3.76, 4.23	2.35	5.7
JRC = 7	3.48, 4.06, 4.64, 5.22	2.90	5.8
JRC = 19	4.20, 4.90, 5.60, 6.30	3.50	7.0

$\tau_1$  the maximum stress in loading–unloading shear pre-stress paths,  $\tau_{cs}$  creep stress,  $\tau_s$  the shear strength in direct shear test

shear stress was applied at a loading rate of 0.5 MPa/min until the sample failed. The shear strength ( $\tau_s$ ) was obtained, and the values are listed in Table 2. The shear strength can be used to determine the shear stress path in subsequent tests.

### 2.3 Test Procedure

#### 2.3.1 Shear Creep Tests with Loading–Unloading Shear Pre-stress Paths

In underground engineering, the excavation process disturbs the surrounding rock mass of tunnels and even adjacent caverns. Loading–unloading–constant loading stress paths are very common in underground engineering. Different loading–unloading shear stress paths lead to differences in the

initial stress and deformation states of the subsequent creep tests and influence the creep characteristics. Engineering stress paths were simulated in our tests and shear creep tests with different loading–unloading shear pre-stress paths were conducted to investigate the influence of the initial states on the creep characteristics. Because the accelerated creep of rock discontinuities is unpredictable and difficult to obtain, especially under complicated stress paths or for samples with small JRC values, the characteristics of accelerated rock discontinuity creep were not considered significant (Wang et al. 2020b). The main aim of this research is to study the influence mechanism of the initial shear stress and shear deformation states on creep. A low creep stress of approximately 50% of the peak shear strength and that was lower than the long-term strength was chosen for the tests. Because only two stages could be observed, the constitutive model of the two stages is relatively simple, which is convenient for analyzing the influence mechanism of the initial states on creep.

In the tests, a normal stress of 6.52 MPa (30% of uniaxial compression strength) was applied to the samples at a loading rate of 0.5 MPa/min and held constant for the remainder of the test. Once the normal deformation had stabilized, shear stress was applied. The loading path of the shear stress was divided into three sections: loading; unloading; and creep (Fig. 3). The shear stress was first loaded to a predetermined stress ( $\tau_1$ ) of approximately 60%, 70%, 80%, and

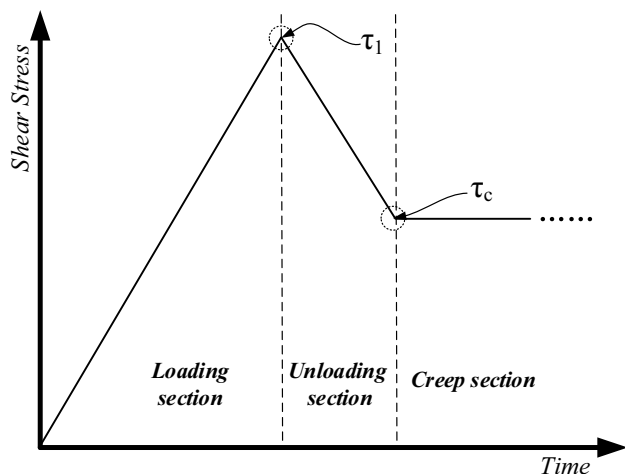


Fig. 3 Stress path of the shear creep tests with loading-unloading pre-stress path

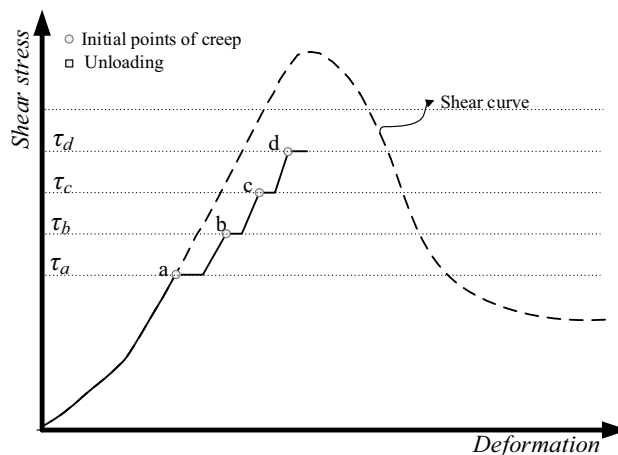
90% of the shear strength, representing the pre-peak stresses in the loading section. The stress was then unloaded to 50% of the shear strength ( $\tau_s$ ) and maintained for 72 h. The actual stress values of the stress paths are listed in Table 2. As a contrast test, creep tests without stress loading-unloading shear pre-stress paths, but only direct application of creep stress values of  $\tau_{cs}$  (listed in Table 2), were conducted.

### 2.3.2 Shear Creep Tests with Different Initial Stress and Deformation States

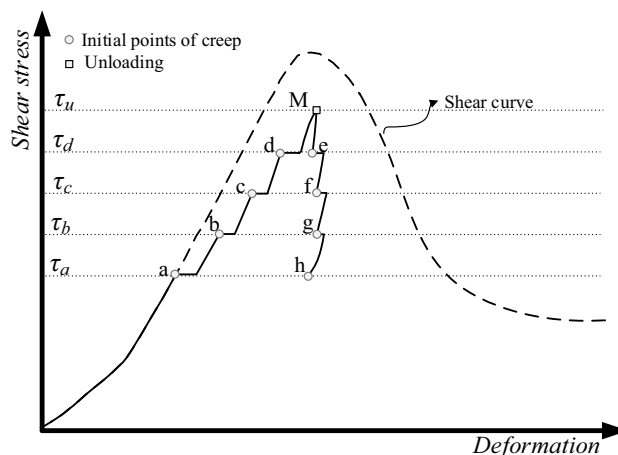
Three tests with different stress paths caused by multi-step creep coupled with loading-unloading stress paths were conducted on samples with  $JRC = 19$  (Barton’s 10th standard profile line) to verify the shear creep test results. A normal stress of 6.52 MPa was first applied to the samples at a loading rate of 0.5 MPa/min and held constant for the remainder of the test. Once the normal deformation had stabilized, the test procedure was as follows (Fig. 4).

Test I: Multi-step shear creep tests were conducted. The stress path is shown in Fig. 4a. Shear stress was applied to a predetermined value and maintained for 72 h. The shear stress was then loaded to a higher value and held constant. The shear creep stresses were 60%, 70%, 80%, and 90% of the shear strength. The corresponding stress paths are shown as a–d in Fig. 4a.

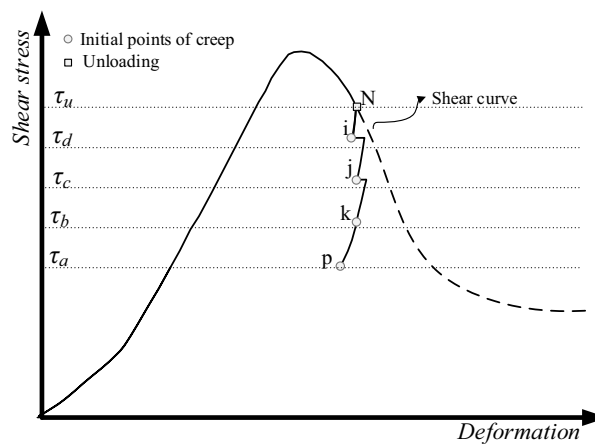
Test II: The shear stress was loaded to point M, which is approximately 95% of the shear strength, under the same four-step creep stress as in test I. The stress on the sample was then unloaded stepwise from point M (Fig. 4b). When the stress reached the predetermined values (e.g., e–h), creep tests were conducted at each point. The creep duration of each step was 72 h. The complete stress path was from a to



(a) Test I



(b) Test II



(c) Test III

Fig. 4 Stress paths of shear creep tests with different initial deformation and stress for a sample with  $JRC = 19$

b to c to d to M to e to f to g to h. The same sample was used for tests I and II.

**Test III:** The tests were conducted after reaching the peak shear strength in the direct shear tests (Fig. 4c). When the shear stress reached N after peak strength, at which point the shear stress was 95% of the shear strength, the shear stress on the sample was unloaded stepwise from point N to the predetermined values at points i, j, k and p, with approximately 10% of the shear strength per step, and creep tests were conducted at each point. The duration of each creep test was 72 h. The actual stress path was a to N to i to j to k to p.

The actual stresses of  $\tau_a$ ,  $\tau_b$ ,  $\tau_c$ ,  $\tau_d$ , and  $\tau_u$  in Fig. 4 were 4.20, 4.90, 5.60, 6.30, and 6.65 MPa, respectively.

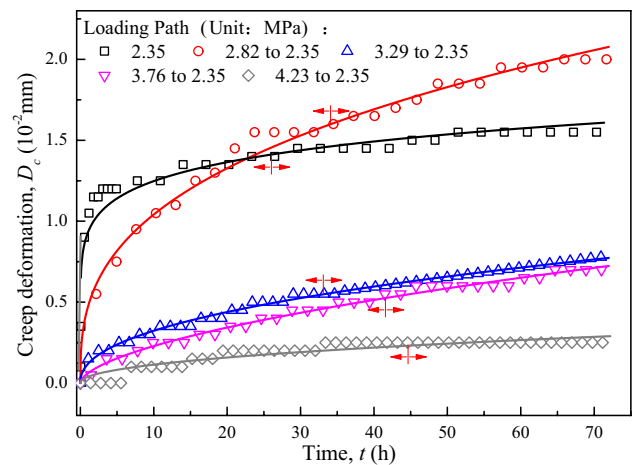
### 3 Results and Discussion

#### 3.1 Shear Creep Tests with Loading–Unloading Pre-stress Paths

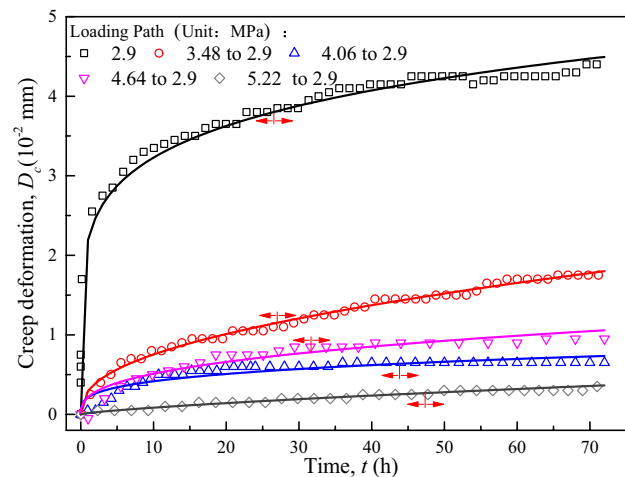
##### 3.1.1 Influence of the Shear Pre-stress Path on the Creep Curve Characteristics of Rock Discontinuities

Figure 5 shows the creep curves influenced by the loading–unloading shear pre-stress path for samples with different roughness values. The creep deformation accumulated with time and the creep rate initially rapidly decreased and then tended to stabilize. The transition creep stage and steady creep stage were observed in all the samples. The tests and characteristics of the creep curves were similar to those of the general creep tests. However, notable changes of the creep curves, including a significant reduction of the creep deformation and variations of some creep characteristics, were observed even under the same creep stress. The creep deformation after 72 h decreased with increasing pre-peak stress ( $\tau_1$ ). The creep deformation was consistently larger when the creep stress was directly applied than with pre-peak stress. Higher pre-peak stress was associated with a smaller difference between the creep curves. For example, when a sample was loaded to 3.5 MPa without pre-peak stress and maintained, the creep deformation reached 0.039 mm over 72 h (Fig. 5c). However, when the sample was loaded to pre-peak shear stresses of 4.9, 5.6, and 6.3 MPa during the loading section and unloaded to 3.5 MPa immediately after applying the pre-peak stress and maintained at 3.5 MPa for 72 h, the creep deformation substantially decreased to 0.0075, 0.0070, and 0.0075 mm, respectively (Fig. 5c). The deformation tended to be nearly the same when the pre-peak stress was larger than 70% of the strength.

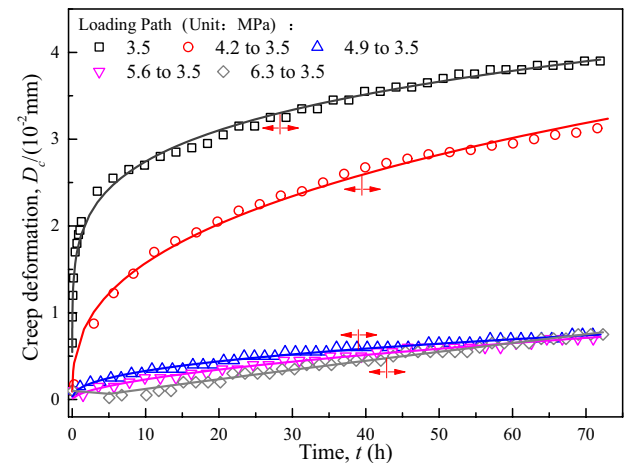
A variation of curve morphology can also be observed in Fig. 5. The duration of the transition creep stage was longer for samples with higher pre-peak stress. The transition



(a) JRC=1,  $\sigma_n=6.52\text{MPa}$



(b) JRC=7,  $\sigma_n=6.52\text{MPa}$



(c) JRC=19,  $\sigma_n=6.52\text{MPa}$

**Fig. 5** Creep curves of the shear tests with loading–unloading pre-stress path ( $\sigma_n$  is normal stress)

points between the transient creep stage and steady creep stage are plotted using “◄►” symbols. The transition point position was determined by the slope variation of the creep curves, in which the slope of the steady creep stage is close to constant. The position of the transition points on the creep curves reflects the duration of the transition creep stage and is closely related to the pre-peak stress. For a creep curve without pre-peak stress or with a smaller pre-peak stress, the transient creep stage is steep and rapidly changes to the steady creep stage, which indicates that the sample has better deceleration ability. However, once the sample experienced the pre-peak stress, not only did the creep deformation decrease but the curvature radius of the creep curve also increased, which indicates the degradation of the deceleration ability of the rock discontinuity and more time in the transient creep stage.

### 3.1.2 Influence of Shear Pre-stress Path on the Creep Deformation of Rock Discontinuities

The creep deformation over 72 h under different test conditions was determined using the data shown in Fig. 5. The relationship between creep deformation and the ratio of the pre-peak stress ( $\tau_1$ ) to shear strength ( $\tau_s$ , which is twice the creep stress  $\tau_{cs}$ ) is shown in Fig. 6. The creep deformation decreases with increasing  $\tau_1/\tau_s$  and follows a bilinear relationship. When the pre-peak stress was less than approximately 70% of the shear strength, the creep deformation decreased with increasing  $\tau_1/\tau_s$ . However, the influence of the loading–unloading pre-stress path on creep deformation was less for samples with pre-peak stress values higher than 70% of the shear strength, and the creep deformation was nearly constant or decreased slightly with increasing

pre-peak stress. There is a threshold at 70% of the shear strength, which is close to the yield stress or long-term stress. When the pre-peak stress was higher than 70% of the shear strength, the cracks in asperities developed unstably, the surfaces tended to be flat, and the block began to slide along the rock discontinuity, because the asperities were sheared off and the grooves were filled (Wang et al. 2018; Wang and Cai 2021). Therefore, the initial JRC of the creep tests tended to be the same after the loading–unloading stress path, the state of cutting and the climbing/sliding asperity also tended to be the same, and the shear creep behavior was identical regardless of the different initial JRC values prior to the loading–unloading stress path. For example, the creep deformation was 0.0025, 0.003, and 0.0075 mm when  $\tau_1$  was 90% of the shear strength for JRC values of 1, 7, and 19, respectively (Fig. 6).

The surface morphology of the rock discontinuities also affects the creep characteristics and loading–unloading pre-stress paths. Creep deformation was larger when  $JRC = 19$  than when  $JRC = 1$  or 7. The influence of the loading–unloading pre-stress path on creep deformation increased with increasing JRC (Fig. 6). For  $JRC = 1$ , the creep deformation was 0.0155 mm when the creep stress was applied to the sample without loading–unloading pre-stress. When the sample was loaded by 4.23 MPa (90% of shear strength), unloaded to 2.35 MPa (50% of shear strength), and maintained, the creep deformation decreased and only 0.0025 mm of deformation was observed after 72 h, demonstrating a reduction of creep deformation by 0.013 mm. However, for  $JRC = 19$ , the creep deformation was 0.039 mm when the creep stress was loaded directly. This deformation decreased to 0.0075 mm when the sample was loaded to 6.35 MPa and unloaded to 3.5 MPa before creep. The creep deformation decreased by 0.0315 mm, which is 2.42 times larger than that when  $JRC = 1$ . The slope of the trend line is largest when  $JRC = 19$  for the sample with a discontinuity. This result indicates that the influence of the shear stress path prior to creep increases with increasing JRC.

The complete curve of the shear creep tests with loading–unloading shear pre-stress paths is plotted in Fig. 7.  $\Delta D$  represents the equivalent plastic deformation caused by cutting and sliding of the contacted asperities, which is irrecoverable during the loading–unloading shear pre-stress path;  $\tau_1$  is the maximum stress in the loading section;  $\tau_{cs}$  is the minimum shear stress in the unloading section and also the creep stress; and  $D_c$  is the creep deformation after 72 h. The relationship between  $\Delta D$  and  $D_c$  in 72 h after the different loading–unloading pre-stress paths was established (Fig. 8). The creep deformation follows a nonlinear relationship with equivalent plastic deformation, which indicates crack growth or the accumulation of equivalent plastic deformation.

With increasing JRC, the shear mode transitions from friction to cutting asperity, and the proportion of plastic

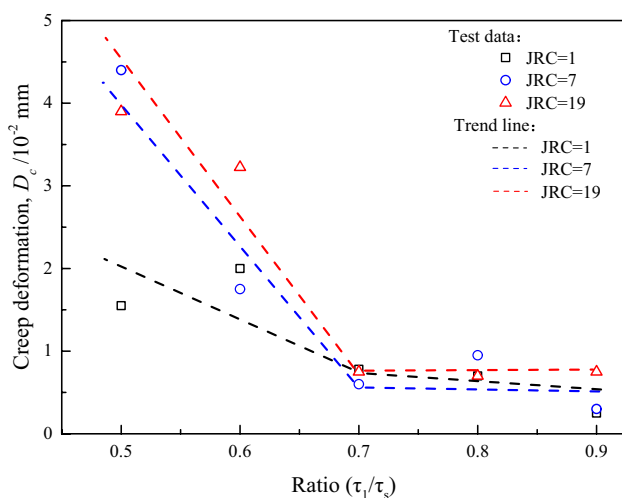


**Fig. 6** Creep deformation with different ratios of pre-peak stress to shear strength ( $\tau_1$  is the peak shear stress in loading–unloading section and  $\tau_s$  is the shear strength which is twice the creep stress  $\tau_{cs}$ )

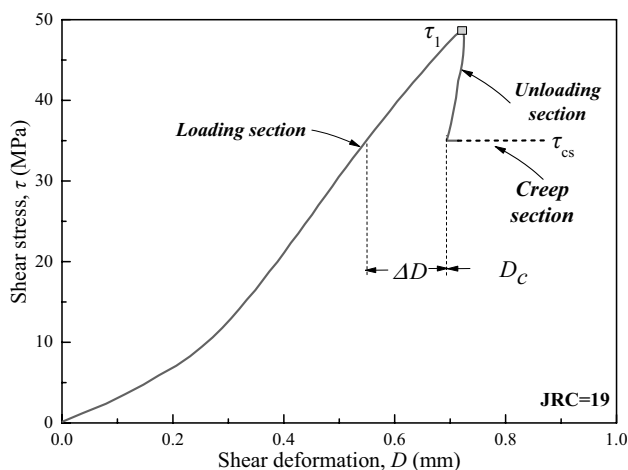
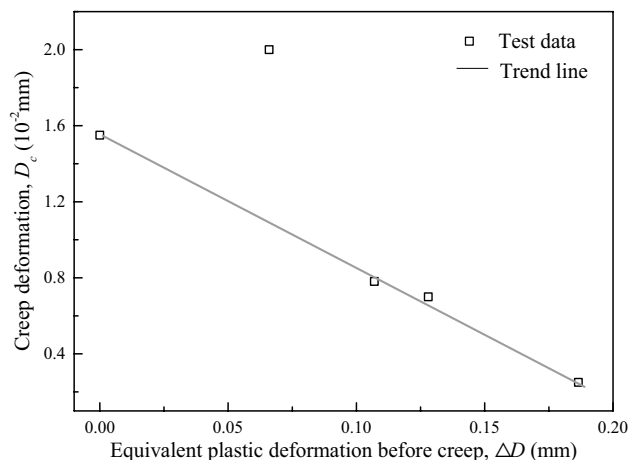


**Fig. 7** Complete curve of the creep tests with loading–unloading pre-stress path ( $\tau_1$  is the maximum stress in the loading section,  $\tau_{cs}$  is the minimum shear stress in the unloading section and also the creep stress,  $\Delta D$  is accumulate plastic deformation before creep,  $D_c$  is the creep deformation in 72 h)

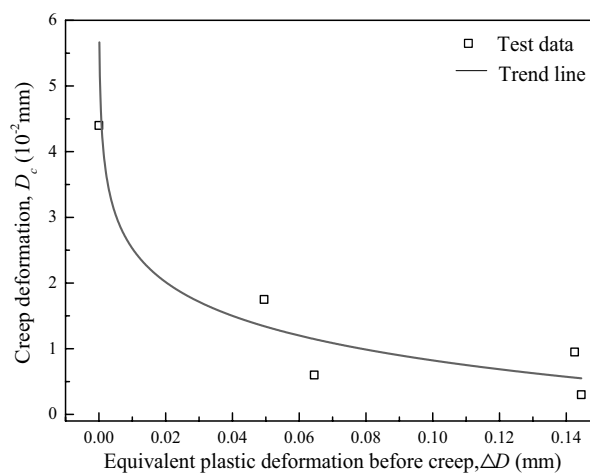
deformation caused by cutting asperity in equivalent plastic deformation increases. This transition is closely related to creep behavior, and increasing plastic deformation results in increasing creep deformation (Wang et al. 2020a, b). However, plastic deformation can be largely consumed by the loading–unloading stress path before creep. The space remaining for creep deformation after the loading–unloading stress path decreased. However, the shearing process during the loading–unloading stress path can lead to decreased JRC and then result in decreased creep deformation (Wang et al. 2018). Therefore, the larger the plastic deformation caused by the loading–unloading stress path, the smaller the creep deformation will be. The influence of  $\Delta D$  on creep deformation also increases with increasing JRC. When  $JRC = 1$ , the shear creep deformation  $D_c$  decreases with  $\Delta D$  and exhibits a linear relationship with a gentle slope, because the cutting asperity is not notable and the plastic deformation caused by the cutting asperity is small. With increasing JRC, the plastic deformation caused by the cutting asperity increases more and the curves become notably nonlinear, first rapidly decreasing and then tending toward horizontal. The nonlinear characteristics of the curve are increasingly apparent with increasing JRC. The test results also illustrate that the creep deformation is greatly influenced by cutting asperities and follows a nonlinear relationship during the shearing process.

**3.1.3 Influence of Loading–Unloading Pre-stress Path on the Creep Rate and Accelerated Velocity**

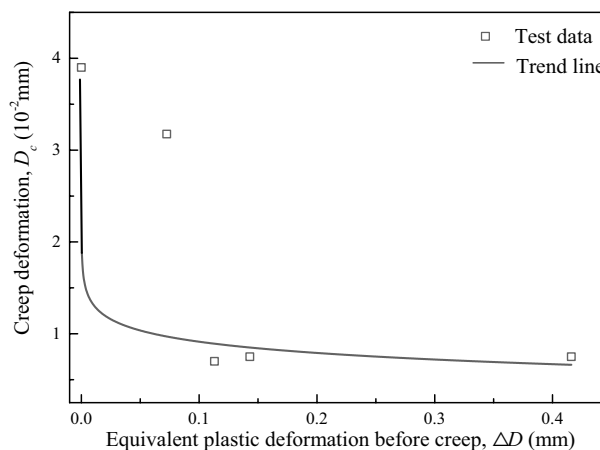
Wang et al. (2020a, b) described creep deformation characteristics by



(a)  $JRC=1, \sigma_n=6.52MPa$



(b)  $JRC=7, \sigma_n=6.52MPa$



(c)  $JRC=19, \sigma_n=6.52MPa$

**Fig. 8** Relationships between creep deformation and the plastic deformation cause by loading–unloading pre-stress path



$$D_c = \frac{m_c}{(n_c + 1)} t^{n_c+1} + v_c t + D_i, \tag{1}$$

where  $t$  is the creep time,  $v_c$  is the creep rate at the end of the steady creep stage,  $m_c$  and  $n_c$  are fitting parameters, where  $n_c < 0$ , and  $D_i$  is the integration constant defined as the instantaneous deformation prior to the shear creep stage. The fitting parameters  $m_c$ ,  $n_c$ ,  $v_c$ , and  $D_i$  can be obtained from the creep curves in Fig. 5.

The shear creep rate can be calculated using the derivative of Eq. (1), given as

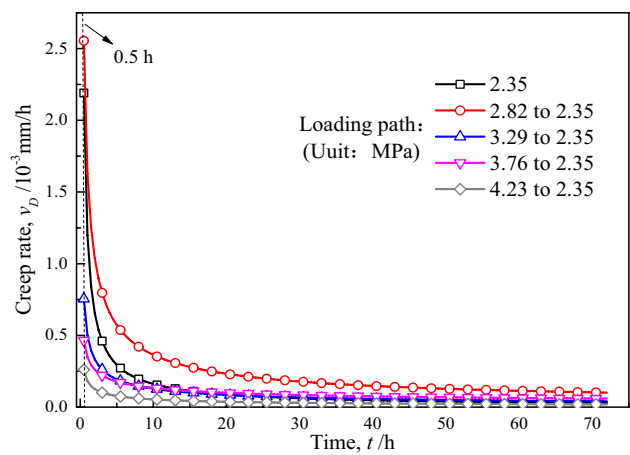
$$v_D = m_c t^{n_c} + v_c, \tag{2}$$

where  $v_D$  is the creep rate. The creep rate curves during the creep tests can be plotted using Eq. (2) and the fitting parameters  $m_c$ ,  $n_c$ , and  $v_c$ . As shown in Fig. 9, the shear creep rate initially decreases very rapidly and the rate of decrease then becomes increasingly low until reaching 10 h, when the creep rate curve tends toward horizontal and is close to zero. The shear creep rate decreases with time and pre-peak stress  $\tau_1$ , which indicates that the shear creep rate is significantly influenced by the loading–unloading pre-stress path. For a creep stress of 2.35 MPa, the shear creep rate at 0.5 h was 8.40 times higher for the sample without loading–unloading pre-stress than the sample with a pre-peak stress of 4.23 MPa (Fig. 9a). Moreover, for samples with creep stress = 2.35 MPa and JRC = 19, the initial shear creep rate was 36.7 times higher in the sample without loading–unloading pre-stress than the sample with a pre-peak stress of 4.23 MPa (Fig. 9c). The influence of the loading–unloading pre-stress path on the creep rate therefore increases with increasing JRC.

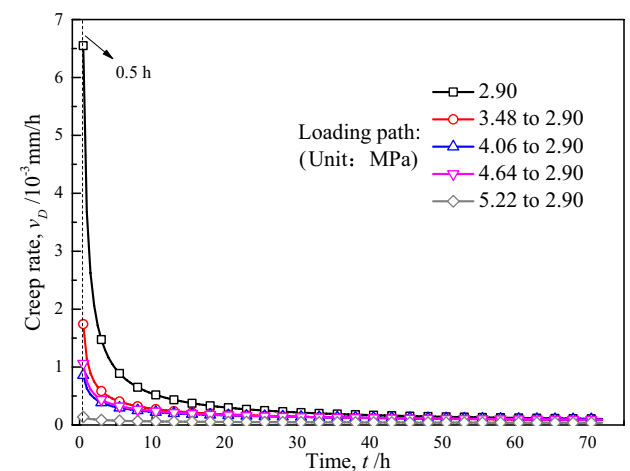
Although the creep is an extremely slow process, when the block slides along the rock discontinuity it still possesses velocity, accelerated velocity, displacement and other kinematic parameters. The accelerated velocity is the bridge connecting mechanics and kinematics. The accelerated velocity during the creep test can be obtained using the second derivative of Eq. (1):

$$a = \frac{d^2 D}{dt^2} = m_c n_c t^{n_c-1}, \tag{3}$$

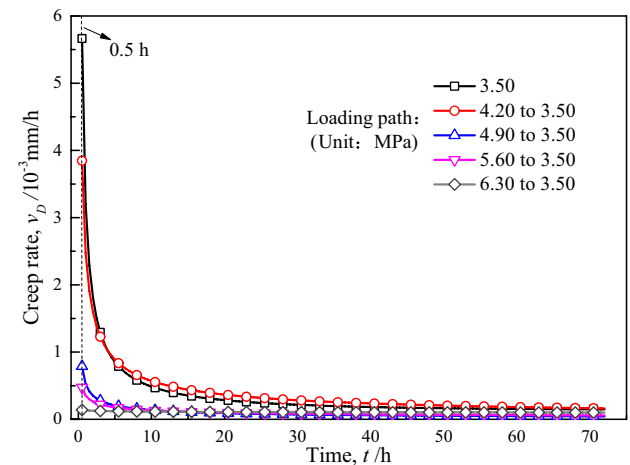
where  $a$  is the accelerated velocity. The variation of accelerated velocity during the creep tests is shown in Fig. 10 using Eq. (3) and fitting parameters  $m_c$  and  $n_c$ . The accelerated velocity decreased very rapidly and tended toward zero within the first hour. The accelerated velocity exhibits a close relationship with the pre-peak stress in the loading section of the tests. Figure 10a shows that the accelerated velocity was consistently higher when the initial creep stress was directly loaded to 2.35 MPa than in the tests with loading–unloading shear pre-stress. The initial accelerated velocity with a



(a) JRC=1,  $\sigma_n=6.52$ MPa

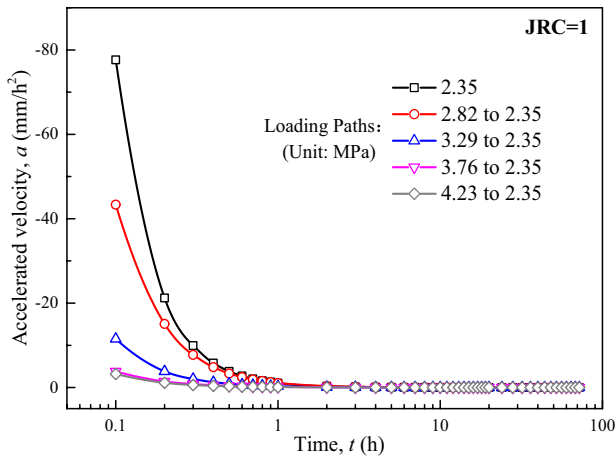


(b) JRC=7,  $\sigma_n=6.52$ MPa

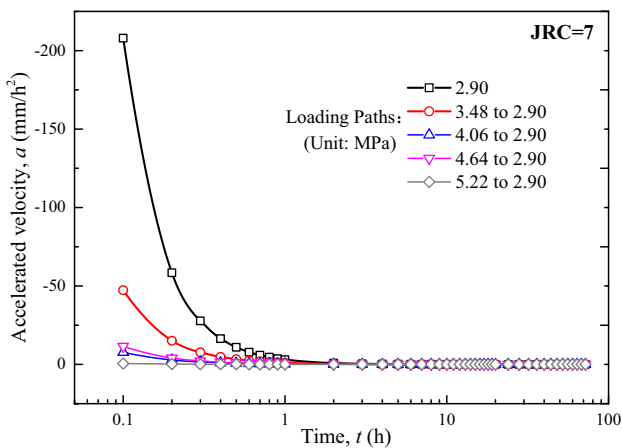


(c) JRC=19,  $\sigma_n=6.52$ MPa

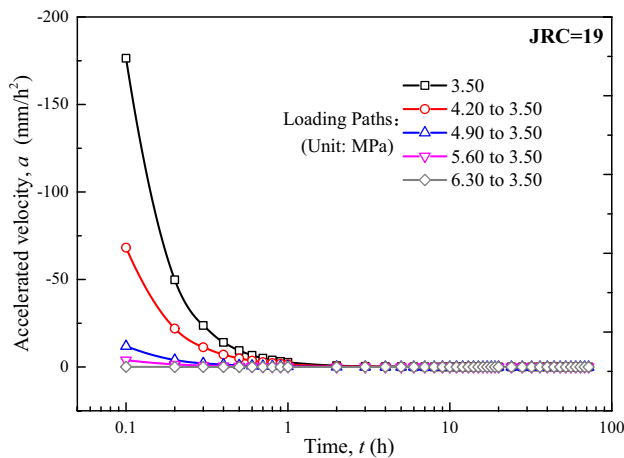
Fig. 9 Creep rate characteristics in creep tests with loading–unloading pre-stress path



(a) JRC=1,  $\sigma_n=6.52\text{MPa}$



(b) JRC=7,  $\sigma_n=6.52\text{MPa}$



(c) JRC=19,  $\sigma_n=6.52\text{MPa}$

**Fig. 10** Accelerated velocity characteristics in creep tests with loading–unloading pre-stress path

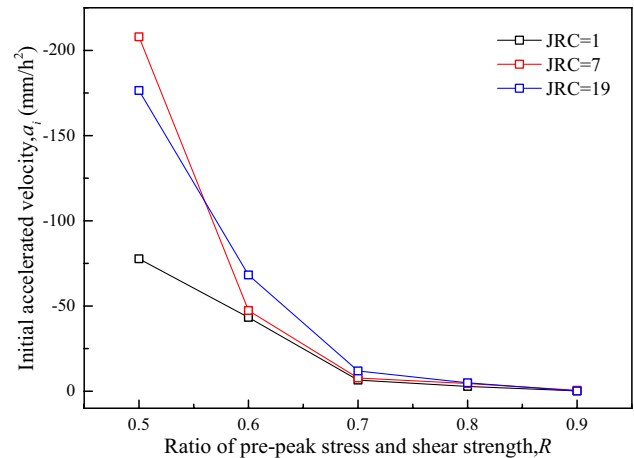


**Fig. 11** Relationships between initial accelerated velocity and ratio of pre-peak stress ( $\tau_1$ ) and shear strength ( $\tau_s=2\tau_{cs}$ )

pre-peak stress of 2.82 MPa (~60% of the shear strength) decreased by less than half of that without pre-peak stress. However, when JRC = 7 or 19, the initial accelerated velocity with pre-peak stress of 3.48 or 4.2 MPa, which is also 60% of the shear strength, decreased by approximately one-fourth of that without pre-peak stress. The influence of pre-peak stress on the initial accelerated velocity is shown in Fig. 11. The initial accelerated velocity decreased with increasing pre-peak stress. It can also be observed that the initial accelerated velocity of samples with larger roughness was consistently greater than for those with smaller roughness for samples treated to loading–unloading pre-stress and under identical pre-peak stress ratio and shear strength conditions. This result indicates that rock discontinuities have a stronger ability to decelerate the creep rate when JRC = 7 and 19. Surface roughness is also an important factor that influences the accelerated velocity. More asperities were sheared during the shear creep tests with increasing JRC, which implies a stronger ability to decelerate the creep rate.

Internal resistance can be investigated in rock discontinuities through their accelerated velocities, which are related to the shear creep rate, crack development, and surface roughness. Accelerated velocities can be used to describe the deceleration ability of rock discontinuities, but cannot be directly monitored in the tests. The internal resistance equation during the creep tests can be written as follows:

$$\tau_c - \tau_i = \frac{ma}{S}, \tag{4}$$

where  $\tau_i$  is the internal resistance in the rock discontinuity that provides the “power” to reduce the creep rate;  $a$  is the accelerated velocity;  $\tau_{cs}$  is the shear creep stress, which is constant in the creep test;  $m$  is the block quality; and  $S$  is the shear area.

According to Eq. (4), the internal resistance is always greater than the creep stress during the creep process because the creep is decelerating motion and the accelerated velocity is negative. According to Eq. (4), the direction of internal resistance is the same as the accelerated velocity, and the development characteristics in the creep tests are consistent with the accelerated velocity. The internal resistance decreased with time during the creep tests as well as with increasing pre-peak stress  $\tau_1$  of the loading section and JRC. The internal resistance to creep stress in the tests that were directly loaded was consistently greater than in those with a loading–unloading pre-stress path. Shear processes (e.g., creep, loading–unloading, direct shear) can all result in crack development or plastic deformation equal to reduced JRC values (Wang et al. 2020a, b). The loading–unloading pre-stress path can therefore result in a reduced JRC, that is, variation of the initial JRC during the creep test. The initial JRC of creep, which is determined by the stress path, decreased with increasing pre-peak stress in the loading section. The internal resistance in the creep tests is, therefore, also related to the initial JRC. Higher JRC values are associated with higher internal resistance.

### 3.2 Mechanism by Which Initial Stress and Deformation Influence Creep Behavior

#### 3.2.1 Shear Creep Tests with Different Initial Stress and Deformation States

The loading–unloading shear pre-stress path influences the initial stress and deformation of subsequent creep and creep characteristics. The creep deformation in each stage is listed in Table 3. Figure 12 is a schematic diagram of the test results that shows the results of tests I, II, and III. Different loading–unloading pre-stress paths lead to different initial stress and deformation of creep and different initial creep positions in the stress–deformation coordinate system, as shown in Fig. 12. The multi-step pre-creep stress path in test I and continuous loading after reaching the shear strength in test II both resulted in the accumulation of plastic deformation prior to creep and thus affected the

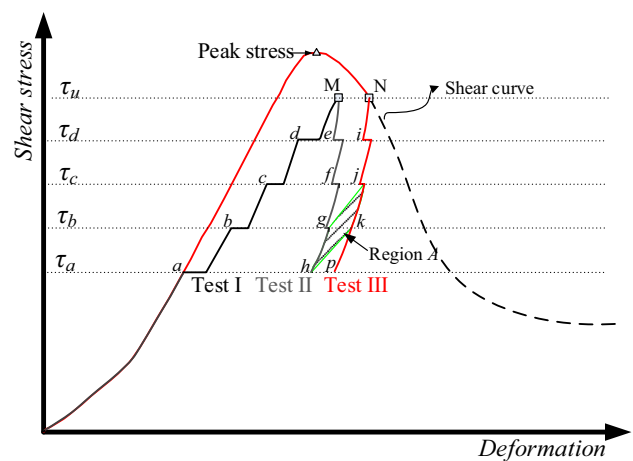


Fig. 12 Schematic diagram of the creep tests with different initial deformation and stress states

creep characteristics. In test II, the creep deformation that begins at point e was largest and decreased sequentially when the creep tests began at points f, g, and h. This pattern was also observed in test III. The creep deformation is strongly influenced by the initial stress or deformation state and decreases when the initial state positions are closer to the lower right-hand corner of the stress–deformation coordinate system, for which the stress is lower and the deformation is higher. For example, when the creep stresses were both 6.3 MPa starting at points d, e, and i (where the degree of deformation was  $d > e > i$ ), the creep deformation was 0.1430, 0.0027, and 0.0015 mm, respectively. The creep deformation in test I was approximately 52 and 95 times higher than those in tests II and III, respectively, even for creep stress values of 6.3 MPa. No creep deformation was observed when the creep began at point h in test II and points k and p in test III, which indicates that the current stress was insufficient to drive the formation of further cracks or plastic deformation in the rock discontinuities and no variation of stress or deformation was observed. In contrast, the stress and deformation could not be maintained when these states were located at points a–g, i, and j.

Table 3 Creep deformation of the shear creep tests with different initial states

Shear stress (MPa)	Test I		Test II		Test III	
	Start point	Creep deformation (mm)	Start point	Creep deformation (mm)	Start point	Creep deformation (mm)
6.3	d	0.1430	e	0.0027	i	0.0015
5.6	c	0.1065	f	0.0019	j	0.0005
4.9	b	0.0745	g	0.001	k	0
4.2	a	0.0555	h	0	p	0

### 3.2.2 Stable and Unstable Regions and Limit Curve in the Shear Stress–Deformation Coordinate System

The test results in Table 3 show time-dependent deformation and that the deformation could not be maintained stably when the creep began at points a–g, i, and j in Fig. 12. These points should thus be regarded as being located in an unstable region of the stress–deformation coordinate system. In contrast, deformation was stable for creep beginning at points h, k, and p and no creep deformation was observed; this area is thus regarded as a stable region. The initial stress and deformation state must therefore be comprehensively considered to assess whether or not a sample will undergo creep, stress relax, or stabilize.

The line dividing the shear stress–shear deformation coordinate system into stable and unstable regions is regarded as the limit curve, as shown in Fig. 13. This curve was first proposed by Bérest et al. (1979) and verified by Goodman (1989), Ge et al. (2003), and Xiao et al. (2010). The limit curve can be defined by the stress–deformation curve when the loading rate is sufficiently slow, or the line at which the creep or stress relaxation stops (Wang et al. 2019). If an initial creep point is located on the limit curve or in the region to the right of the limit curve, as shown in Fig. 13, the corresponding shear stress cannot provide sufficient power to cause the sample to develop new cracks and undergo further plastic deformation.

### 3.2.3 Limit Curve Characteristics

As shown in Fig. 12, the creep deformation in test III was consistently larger than that in test II, even under the same stress level. For the continuous unloading and creep test beginning at point M in test II, the creep deformation was

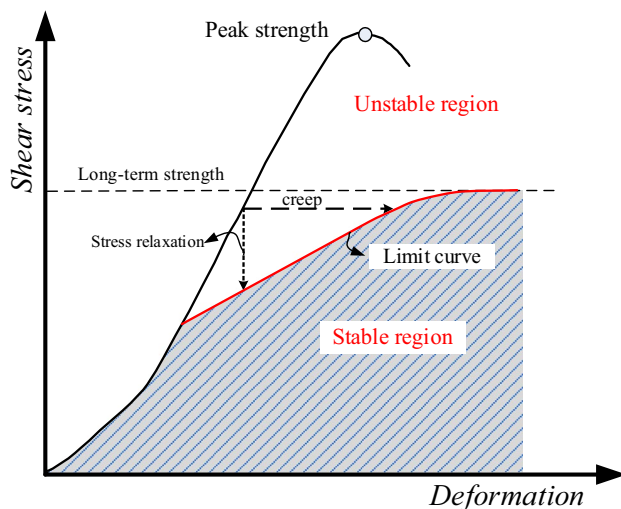


Fig. 13 Stable and unstable regions divided by limit curve

0.001 mm when creep began at point g, at which the initial stress was 4.9 MPa. However, no creep deformation was observed and the sample was stable until the stress unloaded to 4.2 MPa at point h. When the stress was unloaded from point N in test III, the deformation and stress of the sample were stable and no creep deformation was observed at point k, at which the initial stress was 4.9 MPa and the creep deformation was 0. This situation occurred earlier than in test III because the test that began at point k in test III underwent larger deformation prior to creep. Points must therefore exist between points g and h and points j and k on the unloading curve at which there is no creep deformation and the sample remains stable. The limit curve must pass through region A in Fig. 12. Wang et al. (2019) showed that the limit curve is nearly a straight line. Hence, the slope range of the limit curve can be obtained from the range of region A.

### 3.2.4 Speculation Regarding Limit Curve

According to the definition of the limit curve (Fig. 13), when creep stress < long-term strength, the creep or stress relaxation is stopped on the limit curve in Fig. 13 (Bérest et al. 1979). When creep stress > long-term strength, the creep enters the accelerating creep stage and sliding failure occurs. The shear stress–shear deformation curve of the direct shear tests, creep tests, and stress relaxation tests, which have simple stress paths, stop on and do not pass through the limit curve and enter the stable region. Only more complicated stress paths (e.g., loading–unloading stress paths, multi-stage creep tests coupled with loading–unloading stress paths) can produce a shear stress–shear deformation curve that can enter and stop in the stable region.

## 4 Conclusions

This study evaluated the influence of the initial stress and deformation states on the creep behavior of artificial rock discontinuity samples using shear creep tests and the creep mechanism was investigated in detail. Some preliminary results regarding the limit curve and stable and unstable regions were obtained. The conclusions are summarized as follows:

1. The loading–unloading pre-stress path exerted a noticeable influence on the creep behavior in the tests. The creep deformation, creep rate, accelerated velocity, and internal resistance decreased with increasing pre-peak stress  $\tau_1$  in the loading section. Although the basic shape of the creep curve does not change with the pre-stress path, the duration of the transition creep stage signifi-

- cantly increases with increasing pre-peak stress ( $\tau_1$ ) in the loading section.
- Creep behavior is closely related to plastic deformation ( $\Delta D$ ) caused by the pre-stress path. Creep deformation decreases nonlinearly with increasing  $\Delta D$  and the non-linearity becomes increasingly notable for samples with higher JRC values.
  - The loading–unloading shear pre-stress or other pre-stress paths resulted in the accumulation of plastic deformation or crack development, changed the initial stress and deformation states of the creep, degraded the internal resistance and deceleration ability of the rock discontinuity, and changed the overall creep behavior. The influence of pre-stress path on creep deformation is increasingly notable for samples with increasing JRC values because the associated asperities provide more space for creep to occur.
  - The existence of a limit curve is verified and the range of the limit curve slope can be obtained by conducting shear creep tests with different initial deformation and stress states. The limit curve divides the shear stress–deformation space into stable and unstable regions. The sample cannot remain stable if its stress and deformation are located in the unstable region. When the stress is insufficient to drive the formation of further cracks or deformation in the rock discontinuity, the sample remains stable and no creep is observed.

**Acknowledgements** This work was financially supported by the Basic Science Research Program through the National Research Foundation of Korea (NRF) funded by the Ministry of Education (No. 2019R1A6A1A03033167), the National Natural Science Foundation of China (Grant No. 42002266), and the Chinese Postdoctoral Science Foundation (2020M673654).

## Declarations

**Conflict of interest** The authors declare that they have no conflict of interest.

## References

Araki E, Saffer DM, Kopf AJ, Wallace LM, Kimura T, Machida Y, Ide S, Davis E, IODP Expedition 365 shipboard scientists (2017) Recurring and triggered slow-slip events near the trench at the Nankai Trough subduction megathrust. *Science* 356:1157–1160. <https://doi.org/10.1126/science.aan3120>

AsanovPan'kov VAIL (2004) Deformation of salt rock joints in time. *J Min Sci* 40:355–359. <https://doi.org/10.1007/s10913-004-0017-5>

Barton N (1973) Review of a new shear-strength criterion for rock joints. *Eng Geol* 7:287–332. [https://doi.org/10.1016/0013-7952\(73\)90013-6](https://doi.org/10.1016/0013-7952(73)90013-6)

Barton N, Choubey V (1977) The shear strength of rock joints in theory and practice. *Int J Rock Mech Min Sci Geomech Abst* 10:1–54. <https://doi.org/10.1007/BF01261801>

Bérest P, Bergues J, Duc NM (1979) Comportement des roches au cours de la rupture: applications à l'interprétation d'essais sur des tubes épais. *Rev Fr Géotechn* 9:5–12. <https://doi.org/10.1051/geotech/1979009005>

Chen BR, Feng XT, Ming HJ, Zhou H, Zeng XH, Feng GL, Xiao YX (2012) Evolution law and mechanism of rockburst in deep tunnel: time delayed rockburst. *Chin J Rock Mech Eng* 31:561–569

Drescher K, Handley MF (2003) Aspects of time-dependent deformation in hard rock at great depth. *J S Afr Inst Min Metall* 103:325–335

Durrheim RJ, Haile A, Roberts MKC, Schweitzer JK, Spottiswoode SM, Klokow JW (1998) Violent failure of a remnant in a deep South African gold mine. *Tectonophysics* 289:105–116. [https://doi.org/10.1016/S0040-1951\(97\)00310-7](https://doi.org/10.1016/S0040-1951(97)00310-7)

Einstein HH, Veneziano D, Baecher GB, O'Reilly KJ (1983) The effect of discontinuity persistence on rock slope stability. *Int J Rock Mech Min Sci Geomech Abst Perg* 20:227–236. [https://doi.org/10.1016/0148-9062\(83\)90003-7](https://doi.org/10.1016/0148-9062(83)90003-7)

Fernandez LM, Van der Heever PK (1984) Ground movement and damage accompanying a large seismic event in the Klerksdorp district. In: *Proc first int congress rockbursts seismicity min. Johannesburg, vol 22. South Afr Inst Min Metall*, pp 193–198. [https://doi.org/10.1016/0148-9062\(85\)90269-4](https://doi.org/10.1016/0148-9062(85)90269-4)

Gao YF, Huang WP, Qu GL, Wang B, Cui XH, Fan QZ (2017) Perturbation effect of rock rheology under uniaxial compression. *J Cent South Univ* 24:1684–1695. <https://doi.org/10.1007/s11771-017-3575-9>

Ge XR, Jiang Y, Lu Y, Ren J (2003) Testing study on fatigue deformation law of rock under cyclic loading. *Chin J Rock Mech Eng* 22:1581–1585. <https://doi.org/10.1142/S0252959903000104>

Gomberg J, Reasenber PA, Bodin P, Harris RA (2011) Earthquake triggering by seismic waves following the Landers and Hector mine earthquakes. *Nature* 411:462–466. <https://doi.org/10.1038/35078053>

Goodman RE (1989) *Introduction to rock mechanics*. Wiley, Hoboken

Li HB, Feng H, Liu B (2006) Study on strength behaviors of rock joints under different shear deformation velocities. *Chin J Rock Mech Eng* 25:2435–2440. [https://doi.org/10.1016/S1872-1508\(06\)60035-1](https://doi.org/10.1016/S1872-1508(06)60035-1)

Li P, Liu J, Zhu JB, He HJ (2008) Research on effects of water content on shear creep behavior of weak structural plane of sandstone. *Rock Soil Mech* 29:1865–1871. <https://doi.org/10.3901/JME.2008.10.294>

Malan DF (1999) Time-dependent behavior of deep level tabular excavations in hard rock. *Rock Mech Rock Eng* 32:123–155. <https://doi.org/10.1007/s006030050028>

Malan DF, Vogler UW, Drescher K (1997) Time-dependent behaviour of hard rock in deep level gold mines. *J S Afr Inst Min Metall* 97:135–147

Ulusay R (ed) (2015) *ISRM suggested methods for rock characterization, testing and monitoring: 2007–2014*. Springer, New York. <https://doi.org/10.1007/978-3-319-07713-0>

Wang M, Cai M (2021) A simplified model for time-dependent deformation of rock joints. *Rock Mech Rock Eng* 54:1779–1797. <https://doi.org/10.1007/s00603-020-02346-2>

Wang JA, Wang YX, Cao QJ et al (2015) Behavior of microcontacts in rock joints under direct shear creep loading. *Int J Rock Mech Min Sci* 78:217–229. <https://doi.org/10.1016/j.ijrmm.2015.05.002>

Wang Z, Shen MR, Ding WQ, Jang BA, Zhang QZ (2018) Time-dependent behavior of rough discontinuities under shearing conditions. *J Geophys Eng* 15:51–61. <https://doi.org/10.1088/1742-2140/aa83e9>

Wang Z, Gu LL, Shen MR, Zhang F, Zhang GK, Wang X (2019) Shear stress relaxation behavior of rock discontinuities with different joint roughness coefficient and stress histories. *J Struct Geol* 126:272–285. <https://doi.org/10.1016/j.jsg.2019.06.016>

- Wang QY, Liu J, Wang PT, Liu F (2020a) Experimental investigation of accelerated failure of creep rock induced by impact disturbance. *Rock Soil Mech* 313:781–788+798. <https://doi.org/10.16285/j.rsm.2019.0592>
- Wang Z, Gu LL, Zhang QZ, Yue SL, Zhang GK (2020b) Creep characteristics and prediction of creep failure of rock discontinuities under shearing conditions. *Int J Earth Sci* 109:945–958. <https://doi.org/10.1007/s00531-020-01842-8>
- Xiao JQ, Ding DX, Xu G, Jiang FL (2010) Deformation characteristics of rock under constant amplitude cyclic loading. *J Cent South Univ Sci Technol* 41:685–691
- Zhang QZ, Shen MR, Ding WQ (2011) Study on the shear creep characteristics and constitutive model of rock mass discontinuity. *China Civil Eng J* 44:127–132. <https://doi.org/10.1631/jzus.B1000185>
- Zhou H, Meng FZ, Zhang CQ, Lu JJ, Xu RC (2015a) Effect of structural plane on rockburst in deep hard rock tunnels. *Chinese J Rock Mech Eng* 34:720–727. <https://doi.org/10.13722/j.cnki.jrme.2015.04.008>
- Zhou H, Meng FZ, Zhang CQ, Yang FJ, Lu JJ (2015b) The shear failure characteristic of the structural plane and its application in the study of slip rock burst. *Chin J Rock Mech Eng* 34:1729–1738
- Zhu WC, Li SH, Li S, Niu LL (2019) Influence of dynamic disturbance on the creep of sandstone: an experimental study. *Rock Mech Rock Eng* 52:1023–1039. <https://doi.org/10.1007/s00603-018-1642-7>

**Publisher's Note** Springer Nature remains neutral with regard to jurisdictional claims in published maps and institutional affiliations.